AIP | Applied Physics Letters

Micro-pixel light emitting diodes: Impact of the chip process on microscopic electro- and photoluminescence

I. Otto, C. Mounir, A. Nirschl, A. Pfeuffer, Th. Schäpers, U. T. Schwarz, and N. von Malm

Citation: Applied Physics Letters **106**, 151108 (2015); doi: 10.1063/1.4918678
View online: http://dx.doi.org/10.1063/1.4918678
View Table of Contents: http://scitation.aip.org/content/aip/journal/apl/106/15?ver=pdfcov
Published by the AIP Publishing

Micro-pixel light emitting diodes: Impact of the chip process on microscopic electro- and photoluminescence

I. Otto,[1,2,a)] C. Mounir,[3] A. Nirschl,[1] A. Pfeuffer,[1] Th. Schäpers,[4] U. T. Schwarz,[3] and N. von Malm[1]

[1]*OSRAM Opto Semiconductors GmbH, Leibnizstr. 4, 93055 Regensburg, Germany*
[2]*II. Physikalisches Institut, RWTH Aachen University, 52056 Aachen, Germany*
[3]*Department of Microsystems Engineering (IMTEK), University of Freiburg, Georges-Köhler-Allee 103, 79110 Freiburg, Germany*
[4]*Peter Grünberg Institut (PGI-9) and JARA-Fundamentals of Future Information Technology, Forschungszentrum Jülich, 52425 Jülich, Germany*

(Received 30 January 2015; accepted 9 April 2015; published online 16 April 2015)

We investigated the influence of a μ-pixelated chip process on the photoluminescence (PL) and electroluminescence (EL) of a monolithic InGaN/GaN based blue light emitting diode with a continuous n-GaN layer. Particularly, we observed the impact of the metallic p-contact on the PL emission wavelength. A PL wavelength shift in the order of 10 nm between contacted and isolated areas was assigned to screening of internal piezoelectric fields due to charge carrier accumulation. μPL and μEL mappings revealed correlated emission wavelength and intensity inhomogeneities, caused by the epitaxial growth process. The edges of single pixels were investigated in detail via resonant confocal bias-dependent μPL. No influence on the intensity was observed beyond 300 nm away from the edge, which indicated a good working edge passivation. Due to the low lateral p-GaN conductivity, the μPL intensity was enhanced at isolated areas. © *2015 AIP Publishing LLC*.
[http://dx.doi.org/10.1063/1.4918678]

μ-pixelated light emitting diode (μLED) arrays based on III-Nitride semiconductor LEDs are a promising technology for various applications.[1–4] The high efficiency, brightness, reliability, and stability,[5,6] even under harsh temperature conditions, make III-Nitride semiconductor LEDs ideal candidates for many applications in the consumer and automotive area. In combination with a converter and a pixel control unit, these μLED arrays can be used for adaptive front lighting systems (AFS). Today, the pixel size for such systems is in the order of 100 μm. In the future, the requirements regarding resolution of full electronic adaptive drive beams will be even higher. A microscopic investigation of optical and electrical properties of smaller pixels patterned from a commercial monolithic InGaN/GaN based LED structure is therefore of interest. However, due to small pixel size and the homogeneity of electrical and optical properties required for large pixel arrays, μLED arrays cause further challenges. Inhomogeneities of the photoluminescence wavelength and intensity due to quantum well (QW) thickness and indium content fluctuations of InGaN/GaN heterostructures grown by metal organic chemical vapor deposition (MOCVD) had been studied extensively by Chichibu,[7] Vierheilig,[8] and Danhof,[9] amongst others. In conventional LEDs, these inhomogeneities are masked by surface roughening, randomizing light emission across larger chip areas. In the presented pixelated LED, roughening of the GaN surface was avoided to achieve a sufficient low optical crosstalk of neighboring pixels and thereby a high contrast. Consequently, it is of significant importance for μLEDs to study and understand in detail their emission intensity and wavelength inhomogeneities.

In this article, we analyzed the correlation between these inhomogeneities seen through the p-GaN side before and through the n-GaN side after the thin-film chip process. We distinguished between two sources of inhomogeneities: first, the epitaxial growth process; and second, the p-contact influence. Areas with and without p-contact material, which were laterally adjacent to each other, were analyzed. Due to the small lateral distance, there were no significant variations in the epitaxial design. A red-shift of the wavelength at areas with p-contacts was observed and could be attributed to screening of the internal fields. The edge of pixels was studied in detail via bias-dependent μPL and μEL measurements. In isolated areas, the low lateral p-GaN conductivity resulted in an increase of the intensity.

The structures investigated in this work were epitaxially grown on c-plane sapphire substrates by MOCVD. The LED structure consisted of a 4 μm thick n-type GaN buffer layer, an InGaN/GaN multiple QW (MQW) structure, and a Mg-doped p-GaN contact layer with a nominal thickness of 150 nm. The dominant emission wavelength was 450 nm to 460 nm. To study the electro-optical behavior of the μLEDs, two different designs had been used. In both designs, a Ag-based p-contact layer was deposited on the p-GaN surface and structured on pixel level by photolithography and etching. Each pixel was defined by the resulting p-contact area. Arrays with a pixel size down to 5 μm and a pitch down to 10 μm were defined. After structuring the p-contact, its sidewalls were passivated by a 300 nm thick SiO_2 layer (first isolation). For design B, the μLED arrays were additionally dry-etched through the MQWs into the n-type GaN layer. Afterwards, a SiO_2 passivation layer (second isolation) was deposited to prevent current leakage. The passivation layers were opened at the position of the pixels with a photolithography mask and

a)Electronic mail: isabel.otto@osram-os.com

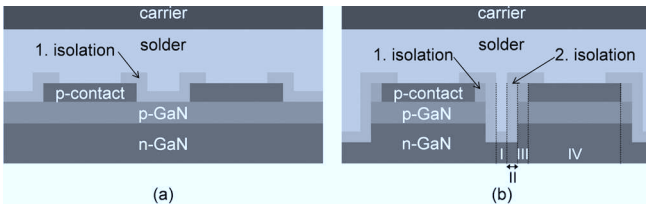

FIG. 1. (a) Design A: cross-section of two pixels defined by the Ag-based p-contact; (b) Design B: cross-section of two pixels defined by the Ag-based p-contact and GaN-etching.

fluorine-based dry-etching. For both designs, a Au-based solder metal was evaporated and the epitaxial layers were bonded to a conductive carrier wafer. To contact the n-GaN, the sapphire was removed by a laser-lift-off process. The chip mesa was etched through the whole GaN layer thickness, and a 600 nm thick SiO_2 passivation layer was deposited on top of the n-GaN surface. Finally, a Au-based bondpad was defined as n-contact by a photolithography step on the n-GaN at the chip edge. Cross-sections of the two different devices are shown in Fig. 1. Each design had a different purpose. Design A, with an unetched active region, was used to study emission intensity and wavelength inhomogeneities on a large length scale, especially wavelength shifts between contacted and isolated areas. With design B, this analysis was not possible because the pn-junction was etched through between the p-contacts. This design was used to analyze the behavior at the pixel edge and the intensity and wavelength fluctuations on a smaller length scale.

The sample with design A was characterized by confocal μPL using a resonant excitation at 375 nm and excitation density of 32 kW/cm^2. An excitation spot size of 0.5 μm in the MQWs was obtained — thanks to an objective with a height numerical aperture of 0.90. A confocal pinhole in the collection optics allowed to achieve a diffraction limited spatial resolution of 300 nm. The setup was carefully aligned by looking at the signal intensity and spectral shift while moving the sample up and down (z-scan). Fig. 2(b) shows the wavelength map of a 50 μm × 50 μm scan area featuring an array of 5 × 5 pixels with 5 μm pixel size and 10 μm pitch. Besides wavelength inhomogeneities, which will be discussed later, a 10 nm red-shift was observed inside the p-contact areas compared to the isolated areas. This wavelength shift was correlated with the spatial characteristic of the intensity (Fig. 2(a)). p-contact areas with a red-shifted emission wavelength had a reduced intensity compared to isolated areas with a shorter wavelength. In the following, we discuss two phenomena which can cause a red-shift of the wavelength at the p-contacts: temperature and shielding of the piezoelectric field. The

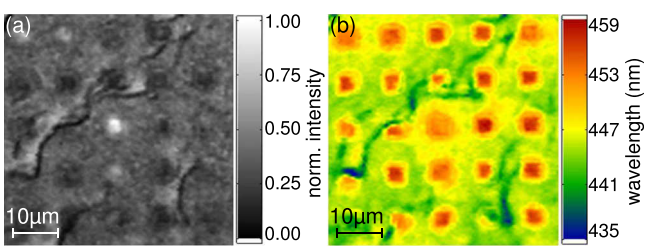

FIG. 2. (a) μPL intensity and (b) μPL wavelength map of a 50 μm × 50 μm area of a μLED of design A at a excitation density of 32 kW/cm^2.

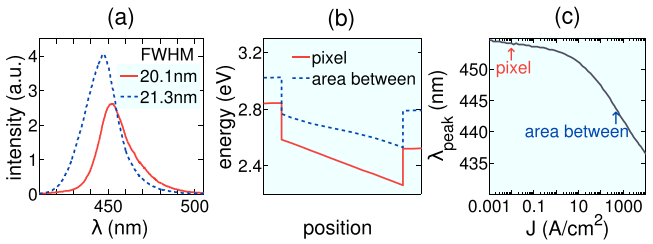

FIG. 3. (a) Measured spectra at a pixel position (solid line) and the area between (dashed line) with the values of the FWHM in the legend. Calculations of the (b) conduction bands (QW) at the pixel and the area between and (c) peak wavelength as a function of the current density.

high excitation power and small spot size of the laser can result in a higher temperature at the p-contacts, because the light is partially absorbed by the Ag. A wavelength shift of 10 nm requires a temperature difference of approx. 150 °C between p-contacts and isolated areas (calculated using Varshni's empirical formula,[10] where the material constants are taken from Vurgaftman[11]). However, the full width half maximum (FWHM) of the spectra would be broadened at higher temperature.[12,13] This was not observed in our measurements (Fig. 3(a)). In these spectra exist no strong resonance effects which can be caused by resonant effects associated with the Ag mirror. The used SiO_2 passivation on top of the n-GaN is too thick to act as anti-reflexion (AR) coating. Yet, the high NA objective causes an angular integration of the spectra, which suppresses Fabry-Perot interferences or resonances stemming from the p-side mirror. Alternatively, the red-shift and decrease in intensity at the p-contacts can be attributed to a different tilting of the energy bands inside the QWs in the p-contacts and the isolated areas, as illustrated by the computation results shown in Fig. 3(b). It is well known that the Quantum Confined Stark Effect (QCSE) due to large polarization fields has a significant impact on the confinement of the charge carriers inside the InGaN QWs. This internal electric field causes the energy bands inside the QW to tilt. At the position of the p-contacts, charge carriers generated by the excitation laser can flow through the contacts to the solder metal. Thus, the amount of charge carriers is relatively low, and the PL intensity is reduced as well. Due to the presence of fewer charge carriers, the internal electric field, induced by the QCSE, is less shielded. Therefore, the QW is more tilted at this position. If the QW is stronger tilted, the energies of the electron and hole wavefunctions are closer together and their overlap is smaller.[14] This results in a longer emission wavelength and smaller emission intensity, respectively. Consequently, the emission wavelength was red-shifted and the emission intensity was reduced at the position of the p-contacts compared to the isolated areas. Between the p-contacts, the p-GaN was isolated against the solder metal. Due to the low p-GaN lateral conductivity, charge carriers were trapped inside the QWs and contributed to the internal electric field shielding. Consequently, the band tilting was reduced and the wavelength was shorter. To support this explanation, Schrödinger-Poisson calculations of the epitaxial layer stack were performed using a lattice temperature of 300 K and band parameters from Vurgaftman.[11] The value of the calculated recombination current density is evaluated regarding the

experimental feasibility. At the position of the p-contacts, we assumed that a significant fraction of the charge carriers generated by the excitation laser flowed into the contacts. In contrast, in isolated areas between the p-contacts, charge carriers were accumulated inside the QWs. For a carrier density n, the recombination current density J can be calculated using the recombination coefficients A, B, and C (fitted elsewhere[15])

$$J = (An + Bn^2 + Cn^3)\frac{qV}{A_{QW}}, \quad (1)$$

where q is the elementary charge, V the total recombination volume, and A_{QW} — the active quantum well area. Fig. 3(c) shows the peak wavelength λ_{peak} dependent on the recombination current density J. To obtain the experimentally observed wavelength shift of 10 nm, a recombination current density of about 200 Acm^{-2} is required. Due to the small spot size and high excitation power of the laser used for the μPL measurements, such high current densities are experimentally feasible. Hence, the explanation of the wavelength shift resulting from areas with different screening of the QCSE is sound.

In Fig. 2, inhomogeneities in the wavelength and intensity map are observed on different length scales. To understand their origin, PL microscope images of the epitaxial wafers at an excitation wavelength of 408 nm were taken before (Fig. 4(a)) and after (Fig. 4(b)) the μLED chip process. An image of the same area under current injection is shown in Fig. 4(c). The inhomogeneities observed before and after the chip process were similar and highly correlated. Thus, these inhomogeneities stem from the epitaxial growth process and not from the p-contacts or processing. In conventional, non pixelated LEDs, these inhomogeneities are masked by roughening the n-GaN light emission surface. Light generated at laterally different positions with different intensity and slightly different wavelength is thereby mixed, and hence, the inhomogeneities disappear. The n-GaN of our μLED was not roughened to avoid optical crosstalk between neighboring pixels, also to facilitate μPL studies. The reasons for these large length scale inhomogeneities are fluctuations in the QW thickness and/or the indium content.[8] For industrial applications of the μLEDs, the intensity has to be more homogenous. This can be achieved with a further development of the epitaxial growth process or by the help of an electronic control unit. Fig. 5 shows resonant μPL mappings at a excitation density of 6.4 kW/cm^2 and a wavelength of the laser of 375 nm and μEL mappings at 2 mA on a 15 × 15 μm^2 pixel of design B, where we selected an area with a most homogeneous PL emission. The scan area was free of the previously discussed large length scale inhomogeneities. A second kind of inhomogeneities was observed, which were on a shorter length scale and were correlated to each other in PL intensity (Fig. 5(a)), PL wavelength (Fig. 5(b)), EL intensity (Fig. 5(c)), and EL wavelength (Fig. 5(d)). Areas with higher intensity corresponded to areas with longer wavelength. The complex physics of carrier localization and redistribution in InGaN QWs, indicated by the correlation of wavelength, intensity, and carrier lifetime, is a central issue in the discussion of internal quantum efficiency of InGaN QWs.[16] The balance between carrier transport, radiative and non-radiative recombination depends among other parameters on carrier density and InGaN QW growth conditions. In the present case, the strong correlation between intensity and wavelength as well as the consistent drop of the intensity of a distance of about 300 nm towards the edge of the μLED pixel (the outer 5% of the pixel area) indicates a considerable redistribution of carriers. Therefore, we explained the correlation as follows: The charge carriers chose the energetically favorable path. They flow therefore preferentially in the long wavelength zones, which have lower energies. Consequently, long wavelength zones contain more candidates for recombination processes, hence their intensity increases.

To get a better understanding of the wavelength and intensity behavior in Fig. 5, we studied the pixel edge under different bias conditions with a resonant excitation at 375 nm. Fig. 6 shows a μPL linescan across the pixel edge, where four different areas are labeled according to Fig. 1(b). Area I was

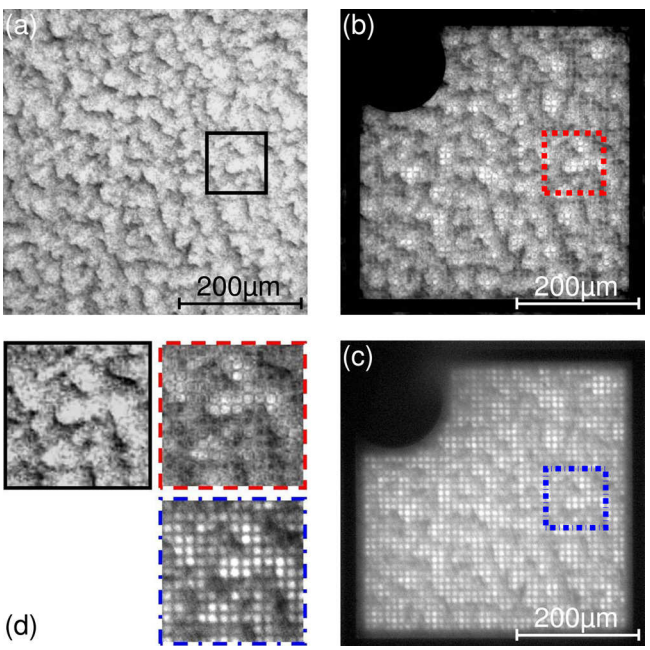

FIG. 4. PL microscope image of a pixel with a size of 8 μm and a pitch of 10 μm from the (a) p-GaN side (before the chip process and without p-contacts; image flipped), (b) n-GaN side (after the chip process), and (c) EL image of the same chip/area. (d) Same images with a higher magnification.

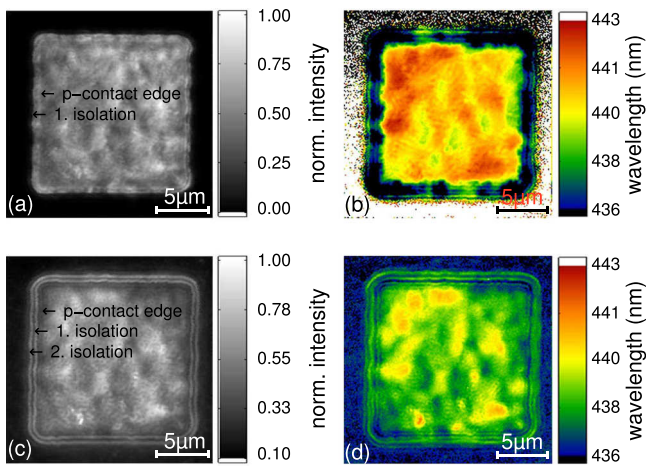

FIG. 5. μPL (a) intensity and (b) wavelength map at I = 0 and 6.4 kW/cm^2; μEL (c) intensity and (d) wavelength at I = 2 mA.

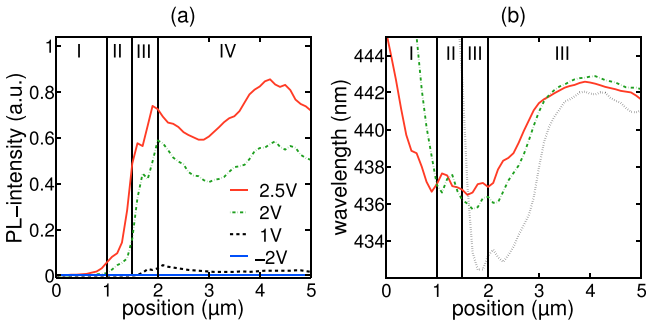

FIG. 6. μPL (a) intensity and (b) wavelength measured under different external bias at a excitation density of 6.4 kW/cm^2 at the edge of a pixel. All data are averaged over 1 μm along the edge.

located outside the pixel and area II labeled the second isolation. No pn-junction existed in both regions. Area III designated the first isolation and area IV the p-contact. Because electron-hole pairs can only be generated in regions with pn-junction, the PL intensity (Fig. 6(a)) dropped off rapidly in area II and I. Therefore, the analysis of the wavelength (Fig. 6(b)) was not meaningful in these regions, i.e., the apparent blue-shift to $\lambda > 440$ nm in region I is an artefact due to varnishing signal intensity. Area III had a pn-junction but no p-contact. Due to the missing contact and the low lateral p-GaN conductivity, the carriers accumulated and shielded the QCSE to a certain extent. Consequently, the PL intensity was increased and the wavelength was blue-shifted compared to area IV where the charge carriers contributed to a current flow through the contact resulting in a red-shifted PL, for the same reason as in Fig. 2. At the position of the p-contact (area IV), the intensity decreased only in the last few hundred nanometers before area III is reached, overlayed by the general intensity fluctuations. As already described in Fig. 5(c), this was an indication of a good working passivation of the pixels. At the border between area III and IV, the intensity was increased due to light extraction at the interface between the isolation and the p-contact. With increasing forward bias, the wavelength difference between region III and IV was decreased. While the laser excitation leads to a carrier accumulation in area III due to the low lateral p-GaN conductivity and the missing p-contact, the carrier concentration was enhanced with increasing forward bias in area IV. The total difference in the amount of charge carriers, which shielded the QCSE, between the isolated edge region (III) and the p-contact area (IV) was decreased. Consequently, the wavelength difference was decreased as well. In area IV, two effects equalized each other. On the one hand, the QWs were more and more tilted with the increase in forward bias. On the other hand, the carrier concentration was enhanced and shielded the QCSE to a certain extent due to the higher bias. The first effect resulted in a red-shifted emission, while the second effect was responsible for a blue-shift (as discussed in Fig. 2). Consequently, at the position of the p-contact, no difference in the wavelength was observed with increasing forward bias. Notice that the intensity under reverse bias was too low to be measured because charge carriers could easily tunnel out of the QW and flow through the contacts. Therefore, the measured wavelength at -2 V is not reported.

In conclusion, we studied the optical properties of a μ-pixelated LED array by means of photo- and electroluminescence. We observed a red-shifted emission in the PL spectra of contacted areas compared to isolated areas. This wavelength shift could be attributed to a larger charge carrier accumulation in the isolated areas which led to a higher screening of the internal piezoelectric field. This explanation was supported by self-consistent Schrödinger-Poisson computations. We observed emission wavelength and intensity inhomogeneities on different length scales in PL and EL mappings. We showed that these inhomogeneities stem from the epitaxial growth process and not from the chip process. Furthermore, we noticed no influence of the chip process on the EL intensity up to 300 nm away from the pixel edge, which indicated a good pixel passivation. These fundamental studies are of significant importance for the further development of μLED arrays and their future industrial applications.

We thank B. Galler, M. Mandl, H. Koch, D. Scholz, C. Vierheilig, D. O'Brien, and M. Peter for fruitful discussions.

[1]H. X. Jiang, S. X. Jin, J. Li, J. Shakya, and J. Y. Lin, "III-nitride blue microdisplays," Appl. Phys. Lett. **78**, 1303–1305 (2001).
[2]V. Poher, N. Grossman, G. T. Kennedy, K. Nikolic, H. X. Zhang, Z. Gong, E. M. Drakakis, E. Gu, M. D. Dawson, P. M. W. French, P. Degenaar, and M. A. A. Neil, "Micro-LED arrays: A tool for two-dimensional neuron stimulation," J. Phys. D **41**(9), 094014 (2008).
[3]J. Day, J. Li, D.-C. Lie, C. Bradford, J. Lin, and H. X. Jiang, "III-Nitride full-scale high-resolution microdisplays," Appl. Phys. Lett. **99**(3), 031116 (2011).
[4]C. Goßler, C. Bierbrauer, R. Moser, M. Kunzer, K. Holc, W. Pletschen, K. Köhler, J. Wagner, M. Schwaerzle, P. Ruther, O. Paul, J. Neef, D. Keppeler, G. Hoch, T. Moser, and U. T. Schwarz, "GaN-based micro-LED arrays on flexible substrates for optical cochlear implants," J. Phys. D **47**(20), 205401 (2014).
[5]G. Stringfellow, "Materials issues in high-brightness light-emitting diodes," in *Semiconductors and Semimetals* (Elsevier, 1997), Vol. 48, Chap I, pp. 1–45.
[6]B. Hahn, B. Galler, and K. Engl, "Development of high-efficiency and high-power vertical light emitting diodes," Jpn. J. Appl. Phys. **53**(10), 100208 (2014).
[7]S. Chichibu, T. Sota, K. Wada, and S. Nakamura, "Exciton localization in InGaN quantum well devices," J. Vac. Sci. Technol. B **16**(4), 2204–2214 (1998).
[8]C. Vierheilig, H. Braun, U. T. Schwarz, W. Wegscheider, E. Baur, U. Strauss, and V. Härle, "Temperature- and excitation density dependency of photoluminescence spectra in InGaN/GaN-heterostructures," Phys. Status Solidi C **4**(1), 179–182 (2007).
[9]J. Danhof, C. Vierheilig, U. T. Schwarz, T. Meyer, M. Peter, B. Hahn, M. Maier, and J. Wagner, "Correlation of surface morphology and photoluminescence fluctuation in green light emitting InGaN/GaN quantum wells," Phys. Status Solidi C **6**(S2), S747–S750 (2009).
[10]Y. Varshni, "Temperature dependence of the energy gap in semiconductors," Physica **34**(1) 149–154 (1967).
[11]I. Vurgaftman and J. R. Meyer, "Band parameters for nitrogen-containing semiconductors," J. Appl. Phys. **94**(6), 3675–3696 (2003).
[12]N. Sarkar and S. Ghosh, "Temperature dependent band gap shrinkage in GaN: Role of electron-phonon interaction," Solid State Commun. **149**, 1288–1291 (2009).
[13]S. M. Sze, *Semiconductor Devices: Physics and Technology*, 3rd ed. (Wiley, 2012).
[14]S. Riyopoulos, "Electrostatically shielded quantum confined stark effect inside polar nanostructures," Nanoscale Res. Lett. **4**(9) 993–1003 (2009).
[15]A. Nirschl, A. Gomez-Iglesias, M. Sabathil, G. Hartung, J. Off, and D. Bougeard, "Quantitative modeling of the temperature-dependent internal quantum efficiency in InGaN light emitting diodes," Phys. Status Solidi A **211**(11), 2509–2513 (2014).
[16]Y. Kawakami, K. Omae, A. Kaneta, K. Okamoto, Y. Narukawa, T. Mukai, and S. Fujita, "In inhomogeneity and emission characteristics of InGaN," J. Phys.: Condens. Matter **13**(32), 6993 (2001).